Design and parameter optimization of air-suction wheel type of seed-metering device with elastic pad for maize

Yuhuan Sun[1], Junhai Guo[2], Linrong Shi[1*]

(1. *College of Mechanical and Electrical Engineering, Gansu Agricultural University, Lanzhou 730070, China*;
2. *College of Mechanical and Electrical Engineering, Lanzhou University of Technology, Lanzhou 730070, China*)

Abstract: Due to the maize growing agronomy requires ground covered by mulch film in the arid zones of the China Northwest region, the seed-metering device must roll over, break the film, and then throw seeds into soil. However, the uneven ground can cause the seed-metering device to shake, reducing seed-metering performance. To improve the adaptability for different shapes of maize seeds, a air suction wheel type seed-metering device with elastic pad was developed for better seed extraction and bump resistance. Firstly, the advantages and influencing factors of the elastic pad were analyzed through four processes of metering seeds. Secondly, the velocity distributions of six diameters of the suction hole are compared to determine the range with FLUENT. Then, a one-factor experiment was conducted to analyze the pattern of the factors (the seed layer height, the critical vacuum, the rotational speed of the seed disk, and the suction hole diameter) influencing the metering seed performance. Finally, a five-level quadratic rotation orthogonal design was used to optimize the parameters. Results show that the optimal values are that the seed layer height is 40 mm, and the critical vacuum is 2.85 kPa, and the rotational speed of the seed disk is 20.1 r/min. The validation experiment resulted in a 93.79% qualified index, with a 4.02% missing index and a 2.19% multiple index.

Keywords: maize seeds, seed-metering device with air suction, elastic suction, parameter optimization
DOI: 10.25165/j.ijabe.20241704.8575

Citation: Sun Y H, Guo J H, Shi L R. Design and parameter optimization of air-suction wheel type of seed-metering device with elastic pad for maize. Int J Agric & Biol Eng, 2024; 17(4): 116–127.

1 Introduction

Maize is the largest grain crop in China, accounting for more than 40% of the country's total grain output and is a matter of food security. Seeding is vital to corn production, and improving seeding quality is crucial to increasing corn yield. The seed-metering device is the core device of the seeder, which can be classified into mechanical and pneumatic types depending on how the seed is taken[1]. The mechanical seeders commonly utilized include the horizontal tray, spoon wheel, and finger clip types. However, they have several problems, such as stringent seed shape and size requirements and susceptibility to seed damage. To overcome these problems, seed-metering devices have been developed and gradually adopted[2]. They comprise the air-suction, air-blowing, air-pressure, and central sets. Given their strong capacity to adapt to various seed shapes and sizes and low damage, air-suction seeders are mainly used for precision seeding[3,4]. It has been the subject of a great deal of in-depth research by scholars at home and abroad. Yang et al.[5] utilize a mechanical seed tray to assist seed suction and fill seed filling by disturbing the seed population. Chen et al.[6] employ the electromagnetic vibration method to reduce transient normal stress between seeds to improve the seed-filling performance of the air-suction seeder. Li et al.[7] conducted a theoretical analysis of the seed-filling process of the vertical tray and found that the main factors affecting the seed-filling performance include vacuum level, suction hole diameter, the rotational speed of the seeding tray, and seed characteristics. Yan et al.[8] found that compared to regular air-suction holes, the shaped hole produces faster airflow velocity and higher air flow density to facilitate seed filling. Yang et al.[9] developed a toothed agitator tray to increase initial seed velocity and disperse the seed population benefits of seed adsorption. Yan et al.[10] A disk chamber synchronized air suction type precision seeder was designed, where the discharging disk and critical vacuum pressure chamber achieve synchronized rotation to avoid the wear of the sealing gasket. Ding et al.[11] developed a cam at the suction hole of the seed suction disk to disturb the seed population and hold the seed to increase the seed filling capacity. In the seed unloading area, they designed a kind of seed unloading wheel that engages with the holes of the seed disk to prevent the holes from being clogged. Tang et al.[12] designed the airflow-assisted seed-dropping device (the seed drop tube) for an inside-filling air-blowing precision seed-metering device. Above research on adopting an air-suction seeder has conducted an in-depth analysis. However, it needs to be fixed to the seeder frame. It is not applied to hole sowing on mulch in Gansu.

Gansu is in the Loess Plateau, with perennial drought and little rain. The geography and climate are harsh, and the film covers cultivation mode so that Gansu grain production year after year harvest[13]. Air-aspirated seed metering device have been widely studied for precision sowing without film covering. However, there are fewer air-suction seeders for metering seed on mulch film. At the same time, the seeder must roll on the film to break the film hole sowing. The unevenness of the ground has a particular effect on the amount of precision seeding. Responding to the above issues, this

Received date: 2023-10-10 **Accepted date:** 2024-06-27
Biographies: **Yuhuan Sun**, PhD student, research interest: Intelligent agricultural equipment research and development, Email: sunyuhuan620105@163.com; **Junhai Guo**, PhD student, research interest: key technologies and equipment for precision seeding in northwest cold and arid zone, Email: 553591864@qq.com.
***Corresponding author: Linrong Shi**, PhD, Associate Professor, research interest: key technologies and equipment for precision seeding in northwest cold and arid zone. Mechanical and Electrical Engineering College, Gansu Agricultural University, Lanzhou 730070, China. Tel: +86-18152092689, Email: shilr@gsau.edu.cn.

study designs an maize air-suction wheel type of seed-metering device with elastic pad. The crucial factors influencing the seed-filling performance and the key components were identified through a force analysis. Fluent was used to analyze the flow field variations of different suction hole diameters. Using the coupled DEM-CFD method, the critical vacuum was determined. The effect of each factor on the metering seed performance was analyzed using a one-factor experiment, while a multi-factor experiment was performed to determine the optimal parameters combination.

2 Materials and methods

2.1 Structure of the seed-metering device

The maize air-suction wheel type of seed-metering device with elastic pad comprised with a seed box, a seed cleaning brush, a seed supply wheel, a seed cleaning tooth, an air chamber baffle, a seeding tray assembly, a duckbill, a rear shell, etc., as shown in Figure 1a. The key core component is a seeding tray assembly on which eight air-suction holes evenly distributed in the circumferential direction, which consists of a seeding tray and an elastic seed suction pad, as shown in Figure 1b. The diameter of the seeding tray is 198 mm, and the thickness is 4 mm. The air-suction hole has a 6 mm diameter hole with a depth of 2 mm and a diameter of 12 mm with a depth of 2 mm. The elastic suction pad, made of elastic rubber, features an outer 12 mm diameter, an inner hole 4 mm diameter (variable), and a depth of 2 mm. It is affixed to the hole of a seeding tray using 6271 adhesives.

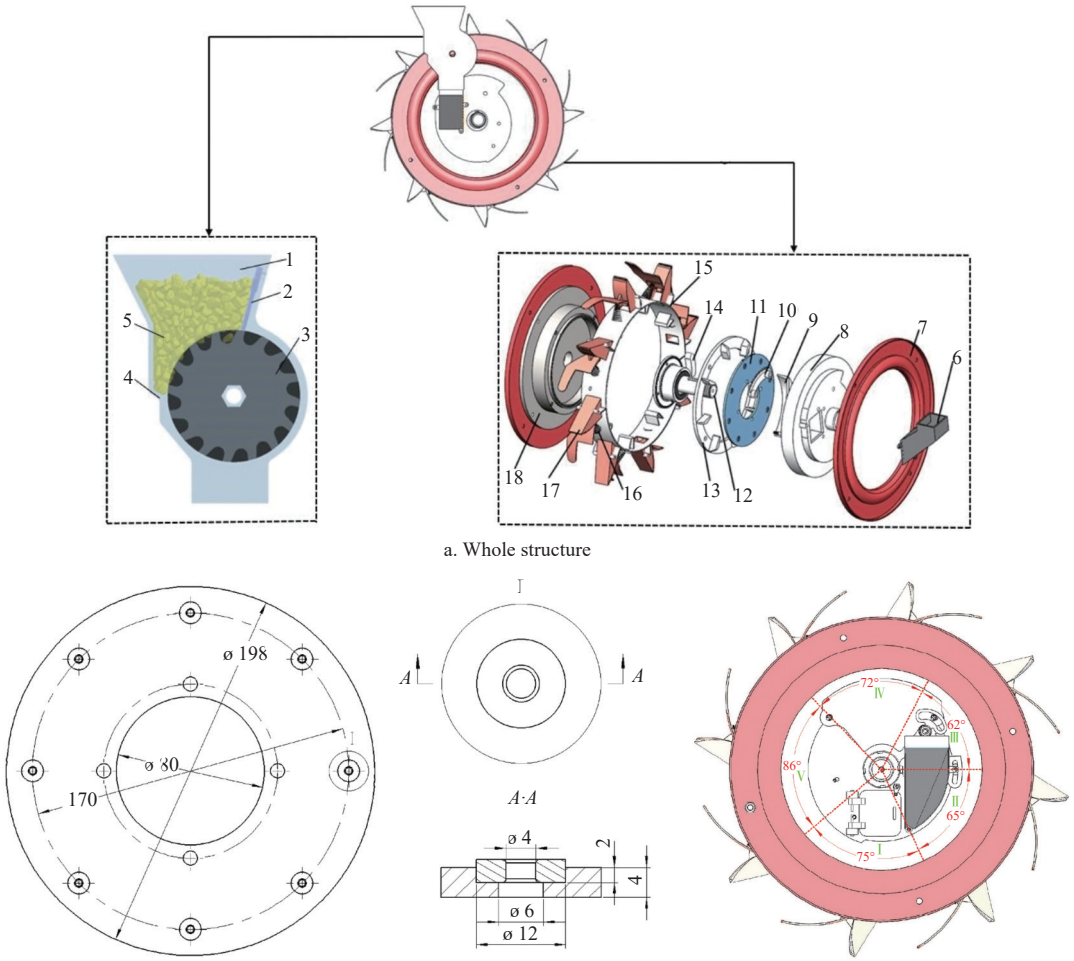

a. Whole structure

b. Structure and size of the seeding tray

c. Functional area division of wheel seed-metering device

1.Seed box 2.Seed cleaning brush 3.Seed supply wheel 4.Shell 5.Maize seeds 6.Seed inlet 7.Front shell 8.Seed chamber spacer 9.Seed spacer 10.Seed cleaning teeth 11.Seeding tray assembly 12.Air tube 13.Seeding tray limit frame 14.Air chamber baffle 15.Duck-bill holder 16.Spring 17.Duckbill 18.Rear shell 19. Seeding tray 20.Elastic suction seed pad Ⅰ.Seed picking area Ⅱ.Seed filling area Ⅲ.Seed clearing area Ⅳ.Seed carrying area Ⅴ.Seed unloading area

Figure 1 Structure of the air-suction wheel type of seed-metering device with elastic pad

According to the working process of metering seeds, the functional area is divided into seed picking area Ⅰ, seed filling area Ⅱ, seed clearing area Ⅲ, seed carrying area Ⅳ, and seed unloading area Ⅴ, as illustrated in Figure 1c. Before working, the air tube connects to a critical vacuum air pump, and the air chamber of the seeder generates a certain critical vacuum. The seed chamber connected to the outside world is a standard atmospheric pressure. The seed in the seed supply device fill into the seed filling area. The seed-metering device rotates on the surface of the mulching film, causing the seeding tray to rotate. Under the action of suction, the corn seeds are adsorbed at the suction holes of the elastic suction seed pad in the seeding tray. In this process, the elastic suction seed pad deforms and has a larger area of adhesion to the seed, while being more airtight, and the seed is more capable of overcoming the seeds resistance. When the seeding tray rotates through the seed clearing area, the seed on the suction holes of the elastic suction seed pad still firmly adsorbed, its surrounding other seeds are cleaned by the seed-cleaning teeth. Then, the seed are steadily transported through the seed carrying area. Upon reaching the seed unloading area, the suction nozzle of the elastic suction seed pad is

blocked. Due to the loss of suction and support, the seed fall in the duckbill by gravity. Finally, the duckbill breaks soil at a certain depth and open and metering the seed into the cavity hole. And so on to complete the hole metering seed.

2.2 Force analysis of seeds metering process

2.2.1 Seeds picking

It is necessary to analyze the seed under force to improve the picking seeds performance of the elastic suction pad. As shown in Figure 2, the seed mass center is taken as the origin, the *x*-axis represents the direction of centrifugal force on seeds, the *y*-axis represents the resistance force from the seed population, and the *z*-axis represents the direction of seed suction. When the seeding tray rotates and works, the maize seed on the elastic suction seed pad supports gravity (G), the adsorption force (F_p), the centrifugal force (J), the other seed resistance force (F_f), the frictional force (f) from the elastic suction seed pad, the support force from the elastic suction seed pad (N). The forces and moments acting on the seed in three directions are balanced, as shown in Equation (1). Comparison of suction seed between rigid and elastic suction pad are seen in Figure 3.

$$\begin{cases} \sum F_x = 0, \ G + J\cos\theta - f = 0 \\ \sum F_y = 0, \ F_f\cos\theta - J\sin\theta = 0 \\ \sum F_z = 0, \ N - F_p = 0 \\ \sum M_O = 0, \ F_p\dfrac{d}{2} - QC = 0 \end{cases} \tag{1}$$

where, θ is the angle between the centrifugal force and the gravitational force, (°); Q is the combined force of G, J, and F_f, N; N is, N; A is the support point; C is the distance from the seed center of gravity to the support point, m; d is the diameter of the suction hole, m.

Combining Equation (1) yields:

$$F_p = \frac{2CQ}{d} = \frac{2C(G + J\cos\theta)}{d} \tag{2}$$

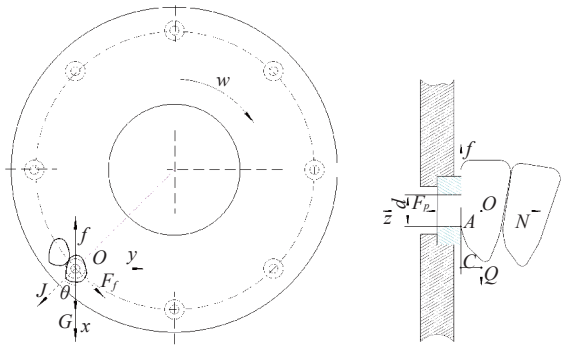

a. Direction of rotation b. Side view

Figure 2 Force analysis of seed filling process

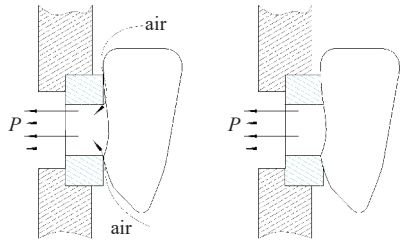

a. Rigid suction pad b. Elastic suction pa

Figure 3 Comparison of suction seed between rigid and elastic suction pad

To ensure that the maize seeds are reliably adsorbed on the elastic suction seed pad, the suction force must vary periodically with the cos φ function. The maximum value is.

$$F_{p\max} = \frac{2C(G + J)}{d} \tag{3}$$

The seed friction between the seed and the contact material determines how firmly the seed is adsorbed. By Equations (1) and (3), it follows that the following equation can express the friction force. Meanwhile, increasing the magnitude of the seed suction force can also increase the seed static friction, as shown in Equation (4), and the suction force can be calculated by Equation (5).

$$f = \mu N = \mu F_p = \frac{2C\mu(mg + mr\omega^2)}{d} \tag{4}$$

$$F_p = PS \tag{5}$$

where, P is the critical vacuum; S is the contact area.

From Equation (4), under the condition that the speed of the seeder is certain, the magnitude of the seed friction is determined by the coefficient of static friction. From Equation (5), increasing the critical vacuum of the seeder and the contact area can increase the suction force on the seed. A comparison of the materials reveals that elastic rubber has better friction characteristics and force deformation compared to steel.

From Figure 3, as the rigid suction nozzle is not easy to deform, the seed in the suction nozzle is hollow, and the air is sucked into the air chamber, resulting in a lack of vacuum. In contrast, with an elastic suction pad by the seed suction, the deformation of the seed contact fit, the air cannot enter the air chamber. At the same time, the suction holes indirectly increase the size of the seed suction and improve the seed suction force.

2.2.2 Seeds clearing

From the above analysis, the elastic seed suction pad could deform by force, the ability to adsorb seeds is more vital, the chance of air leakage is smaller, and the opportunity for multi-grain adsorption is smaller. Even if the adsorption of multiple seeds, with the elastic pads of the suction disk seed clearing effect, is better than the traditional suction disk. In this paper, the seed-clearing teeth are used to clean the seeds at the suction hole by continuous collision to complete the seed clearing and the force analysis of the seeds in the seed clearing teeth clearing area, as shown in Figure 4. Seeds adsorbed by the suction hole with the seed disk with an angular velocity ω clockwise rotation, with the center of the suction hole as the origin to establish a coordinate system, the *x*-axis is positive for the positive direction of the centrifugal force on the seeds, the *y*-axis is positive for the perpendicular centrifugal force and clockwise direction, the *z*-axis is positive for the critical vacuum adsorption of seeds in the direction of the adsorption force. Seeds are subjected to

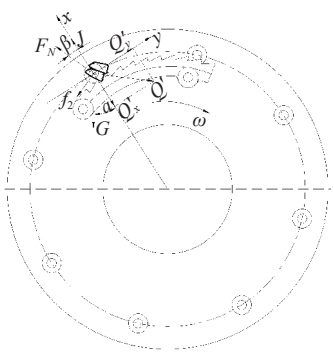

Figure 4 Force analysis of the seed-clearing process

suction hole adsorption force F_p, seed disk centrifugal force J, suction hole support force N, its gravity G, the seed clearing teeth on the seed support force F_N, friction on the seed f_2, the seed disk on the seed support force N, friction on the seed f, where Q is the combined force of G, J and F_N for the combined force Q of the opposite force, the size of the same, the direction of the opposite.

To ensure that the dominant adsorption of the seed does not fall, the negative vacuum on the seed adsorption force should be greater than the force required for the seed to fall. The seed force needs to reach equilibrium. The seed force and moment in three directions should be 0, **a**s shown in Equation (6).

$$\begin{cases} \sum F_x = 0, \ J + F_N cosB - Q'_x - Gcos\alpha - f_2 sinB = 0 \\ \sum F_y = 0, \ Q'_y - F_N sinB - f_2 cosB - Gsin\alpha = 0 \\ \sum F_z = 0, \ F_p - N_z = 0 \\ \sum M_a = 0, \ F_p \dfrac{d}{2} - QC = 0 \end{cases} \tag{6}$$

where, $f_2 = \mu_1 F_N$; α is the angle between the gravity force G on the seed in the x-direction, (°); β the angle between the support force F_N on the seed by the seed-cleaning teeth and the centrifugal force J on the seed disk, (°); and μ_1 is the friction factor between the seed and the seed-cleaning teeth.

From Equation (6), we can get:

$$F_p = \frac{2C}{d} \cdot \sqrt{\left[J + F_N(\cos\beta - \mu_1 \sin\beta) - G\cos\alpha\right]^2 + \left[F_N(\sin\beta + \mu_1 \cos\beta) + G\sin\alpha\right]} \tag{7}$$

From Equation (7), under the condition that other settings define certain conditions, the demand seed stabilization adsorption force is positively correlated with the support force of the seed-clearing teeth on the seed F_N, under the condition that the critical vacuum is certain. The seed adsorption force is specific. Increasing the support force of the seed-clearing teeth on the seed can destroy the non-adsorption dominant seed adsorption state and then be removed. At the same time, the adsorption of superior seeds due to the elastic suction nozzle adsorption, the anti-vibration ability is better, the support force of the teeth of the seed clearing can be adjusted to adjust the attitude of the seed, and the adsorption effect is better.

2.2.3 Seeds carrying

When the seed rotates with the seed disk to reach the seed carrying area, there is less interaction between the seeds and between the seeds and the seed clearing plate, and the forces on the seeds, as shown in Figure 5.

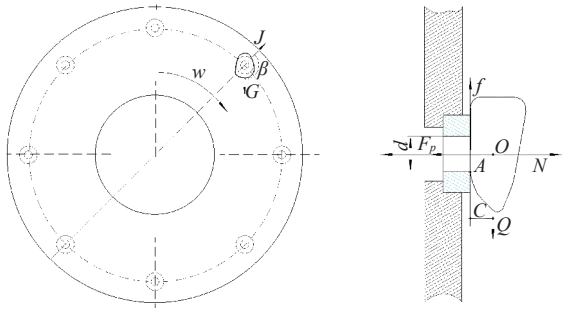

a. Direction of rotation b. Side view

Figure 5 Force analysis of the seed carrying process

Establish a system of equations for the balance of forces on the seed, as shown in Equation (8).

$$\begin{cases} \sqrt{G + J + 2GJ\cos\beta} = f \\ QC = \dfrac{d}{2} F_p \\ N = F_p \end{cases} \tag{8}$$

where, β is the angle between gravity G and centrifugal force J, (°).

Simplifying Equation (8) gives that.

$$F_p = \frac{2CQ}{d} = \frac{2C\sqrt{G + J + 2GJ\cos\beta}}{d} \tag{9}$$

From Equation (9), the theoretical adsorption force in the seed-carrying area is smaller than the theoretical value in the seed-picking area, so if we can ensure that the seed-absorbing section has a stable critical vacuum, we can realize the stable seed-carrying. Due to the elastic air-absorbing cushion connection between the seed and the suction disk, the vibration generated by the seed dispenser rolling on the ground is filtered by the air-absorbing cushion and transferred to the seed, ensuring seed-carrying stability.

2.3 Determination of key factors

2.3.1 Structure of the seeding tray

The seeding tray is critical in seed suction, including picking, clearing, carrying, and unloading. A larger seeding tray diameter allows for more suction holes. However, the diameter is related to the overall structure of the seed-metering device[13,14], typically ranging from 140 to 260 mm. A diameter of 198 mm has been determined. Based on the agronomic requirements in the China northwestern region, maize should be planted at a spacing of 220 mm and a depth of 50 mm. Equations (10)-(12) can be used to calculate the linear speed of the seeding tray.

$$v_p = \frac{\pi d_p \omega}{60} \tag{10}$$

$$n_p = \frac{60 v_m}{S Z_p} \tag{11}$$

$$Z_p = \frac{\pi(D_p + h_p)(1 + \delta)}{i_p S} \tag{12}$$

where, v_p is the linear speed of the seeding tray, m/s; d_p is the diameter of the seeding tray, m; n_p is the rotational speed of the seed disk, r/min; Z_p is the number of suction holes; D_p is the diameter of the ground wheel, assumed to be 0.37 m; h_p is the planting depth; δ is the slip coefficient of the ground wheel, supposed to be 0.057[15]; i_p is the transmission ratio, assumed to be 1.

From Equation (12), the number of suction holes (Z_p) is calculated to be 6.34. From Equations (10) and (11), when the plant spacing (S) and the operating speed (v_m) are constant, increasing Z_p can decrease v_p and ω, improving the seed-filling performance. Thus, Z_p is selected to be 8. The diameter of the suction hole (d) can be calculated as follows.

$$d = (0.64 \sim 0.66)b \tag{13}$$

where, b is the average width of the maize seed, mm.

From Equation (13), as the maize's average width is 8.72 mm, d is selected as 5.58 mm, and the diameter of the suction hole is 5.5 mm. Typically, the suction hole is located 10-20 mm from the edge of the seeding tray. The radius of the suction hole circumference is designed to be 85 mm.

2.3.2 The diameter range of the suction hole

Six different diameters (3.5 mm, 4 mm, 4.5 mm, 5 mm, 5.5 mm,

and 6 mm) were simulated using Fluent to determine the diameter range of the suction hole. The internal flow field was modeled with Solidworks, as shown in Figure 6a. The model was imported into ICEM-CFD for unstructured meshing, as illustrated in Figure 6b. A non-implicit solver is selected with the standard *k-ε* turbulence. The suction hole region is defined as mesh motion, and the rotational speed is set to 20 r/min. The inlet is specified as a 0 kPa pressure inlet, while the outlet is a 3.5 kPa pressure outlet. The suction hole wall is assigned a moving wall, while the rest is subjected to a no-slip model. The convergence condition is set at 1×10^{-4}, and the time step is 1000 with the duration of 1×10^{-4} s. The total simulation time is 0.1 s.

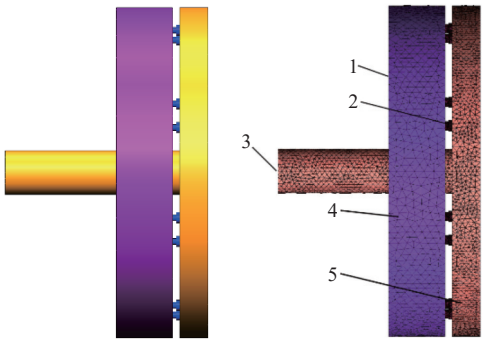

a. 3D model b. Unstructured mesh model

1. Inlet 2. Suction hole 3. Outlet 4. Seed filling area 5. Vacuum area.

Figure 6 Simulation model of the flow field

To investigate the flow field variation caused by the suction hole diameters, the velocity distributions in the suction holes are compared in detail. The pressure distributions are shown in Figure 7.

From Figure 7, we know that as the suction hole diameter increases, the velocity distributions in the suction hole first increases and then decreases. The maximum value is observed when the diameter is 4.5 mm.

2.4 Determination of critical vacuum

To determine the critical vacuum of five different shape types of maize seeds, a experiment was conducted with the EDEM-FLUENT coupling method. A simulation model is required, including a seeds model and a seed-metering device.

2.4.1 Maize seed

Zhengdan 958 was selected as the experiment material. Due to a combination of genetic and environmental influences, maize grows in different shapes at different locations on the cob. Maize seeds shape are broadly classified into five types (horse tooth, spherical cone, spherical, irregular, oblate), as shown in Figure 8a, In triaxial dimension, their length (*L*), width (*W*) and thickness (*T*) are listed in Table 1. 1000 seeds were randomly taken for shape counting, and the results show that 387 seeds are horse tooth, and 174 seeds are spherical cone, and 288 seeds are spherical, and 109 seeds are irregular, and 42 seeds are oblate. With the help of Solidworks, the three-dimensional model of five shape types was modeled[16], as shown in Figure 8b. Since the particle volume is required to be less than the grid volume in the gas-solid coupling process, according to the minimum volume of the flow field grid (1.68×10^{-9} m^3), the radius of the filled particles was determined to be 0.5 mm (volume 5.24×10^{-10} m^3), multiple small spherical particles are stacked and bonded together, as shown in Figure 8. Bond parameters are that normal stiffness per unit area is 1×10^8 N/m^3, and shear stiffness per unit area is 5×10^7 N/m^3, and critical normal stress is 1×10^{30} Pa, and critical shear stress is 1×10^{30} Pa, and the bond radius is 1.5 mm. The process of particle replacing and bonding is illustrated in Figure 9.

2.4.2 Seed-metering device

Due to the judgment of adsorption seed critical pressure vacuum, the seed inlet, seed cleaning teeth, seed tray limit frame, seed separator, rear shell, air tube, duckbill, and other parts in the simulation process do not play a role, the seed-metering device model with the suction hole diameter 5 mm was simplified, as shown in Figure 10.

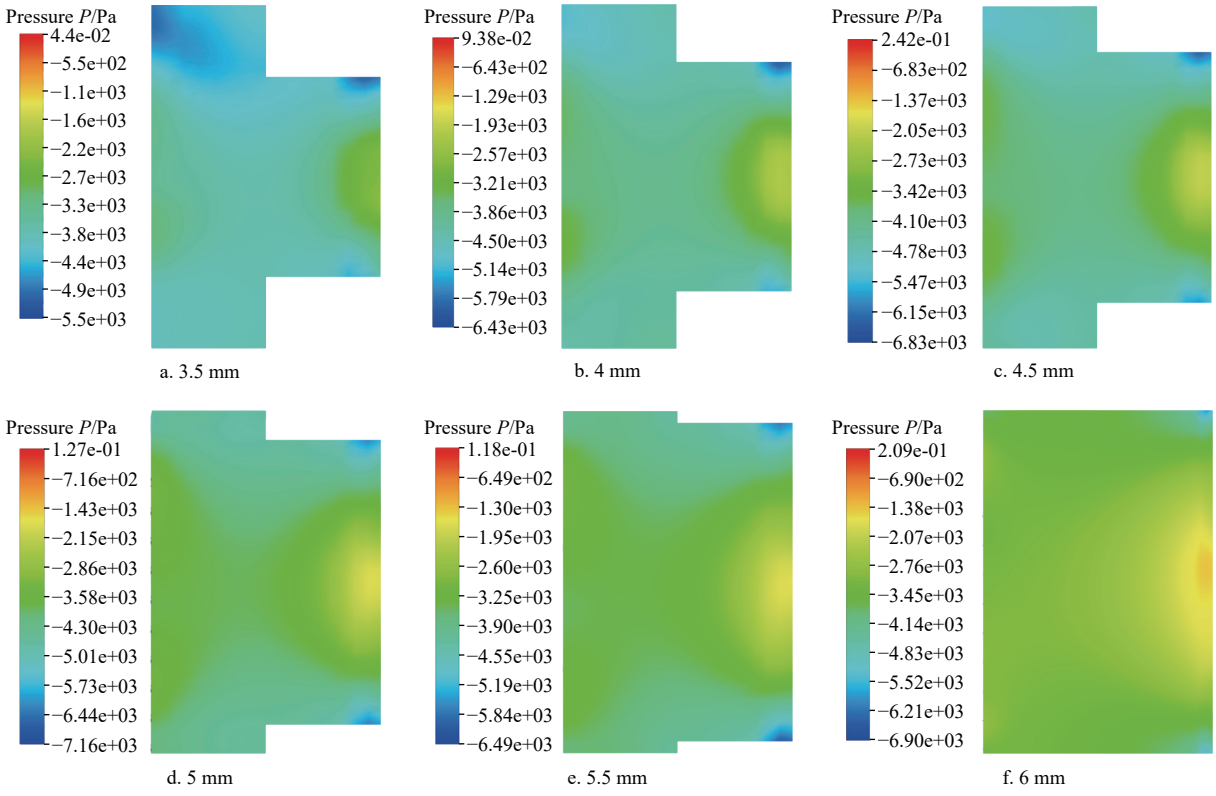

a. 3.5 mm b. 4 mm c. 4.5 mm

d. 5 mm e. 5.5 mm f. 6 mm

Figure 7 Pressure distributions in the suction hole

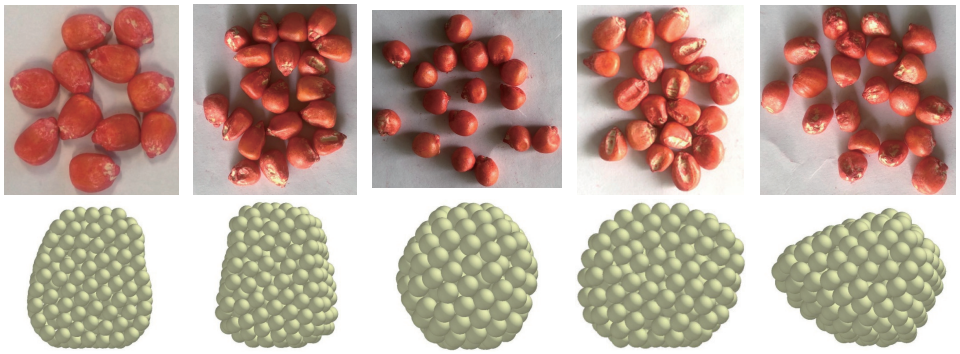

a. Horse tooth b. Spherical cone c. Spherical d. Oblate e. Irregular

Figure 8 Simulation model of maize seeds

Table 1 Maize triaxial dimensions

Value	Horse tooth			Spherical cone			Spherical			Oblate			Irregular		
	L	*W*	*T*	*L*	*W*	*T*	*L*	*W*	*T*	*L*	*W*	*T*	*L*	*W*	*T*
Max.	13.00	10.74	8.86	12.62	10.32	9.30	10.86	9.84	8.63	12.83	10.94	5.53	12.11	10.98	9.63
Min.	9.39	7.19	3.84	7.42	6.75	4.46	7.15	6.70	6.30	8.29	7.96	4.18	7.21	6.29	5.02
Mean	11.64	8.95	4.65	10.42	8.38	6.72	9.15	8.33	7.60	10.98	9.03	5.53	9.06	8.91	7.82
S.D.	0.63	0.69	0.44	1.06	0.65	0.72	0.68	0.48	0.67	0.79	0.70	0.61	1.52	0.97	1.21

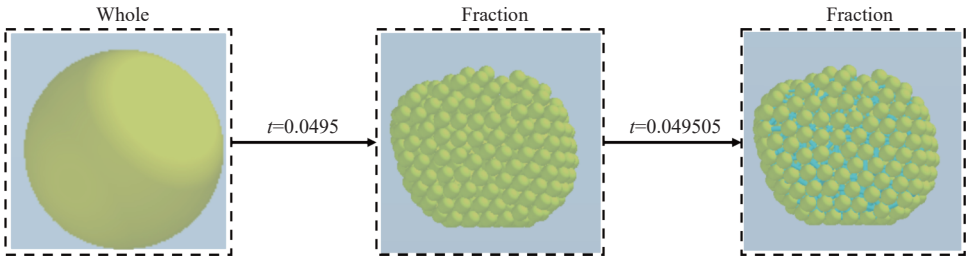

Figure 9 Particle replacement bonding process

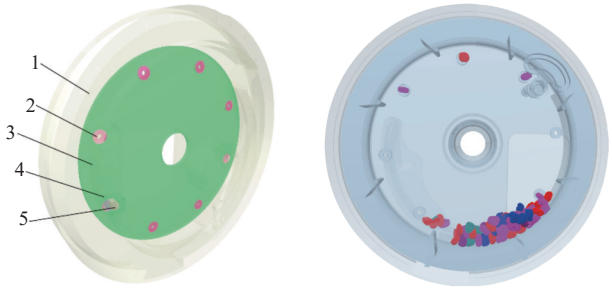

a. Structure Composition b. Maize in seed metering device

1.Front shell 2.Elastic seed suction pad 3.Seeding tray 4.Particle factory 5.Maize seed.

Figure 10 Simulation model of the seed-metering device

2.4.3 Simulation parameters

The simulation metering seed process requires setting relevant parameters, as shown in Table 2. The time step in EDEM was set to 1×10^{-5} s, while that in Fluent was set to 5×10^{-4} s. Only a seed model was generated at the location above the suction hole to optimize computational efficiency. Data were saved at 0.01 intervals with a total duration of 0.2 s. The drag force exerted on the horse tooth seed model is analyzed under critical vacuum conditions (1.5 kPa, 1.6 kPa, 1.7 kPa and 1.9 kPa), as shown in Figure 11. As the adsorption effect varies with the seed shape, the drag force exerted on different seed model (oblate, horse tooth, spherical cone, irregular, spherical) are compared when the critical vacuum is 1.6 kPa, as shown in Figure 12.

2.4.4 Effect of critical vacuum on carrying seed process

To explore the critical vacuum conditions under which the maize kernels remain stable during the rotation of the seed suction disk, the adsorption process only overcoming gravity by the seed suction disk was investigated by gas-solid coupling simulation. When the critical vacuum changed from 1.5 to 1.7 kPa, the falling processes of the horse tooth shape maize kernels in the distance from the seed suction disk distance of 2 mm near the generation were observed as shown in Figure 11.

Table 2 Simulation parameters in EDEM

Project	Parameter	Value	Source
Maize seed	Poisson's ratio	0.4	[17]
	Density/(kg·m^{-3})	1 196	[17]
	Shear modulus/Pa	1.37×10^{8}	[17]
Steel	Poisson's ratio	0.28	[18-19]
	Density/(kg·m^{-3})	7 850	[18-19]
	Shear modulus/Pa	8.1×10^{10}	[18-19]
Rubber	Poisson's ratio	0.4	[20]
	Density/(kg·m^{-3})	1 500	[20]
	Shear modulus/Pa	1×10^{8}	[20]
Maize-maize	Coefficient of restitution	0.182	Experiment
	Coefficient of static friction	0.121	Experiment
	Coefficient of rolling friction	0.024	Experiment
Maize-steel	Coefficient of restitution	0.587	Experiment
	Coefficient of static friction	0.392	Experiment
	Coefficient of rolling friction	0.143	Experiment
Maize-rubber	Coefficient of restitution	0.611	Experiment
	Coefficient of static friction	0.627	Experiment
	Coefficient of rolling friction	0.170	Experiment

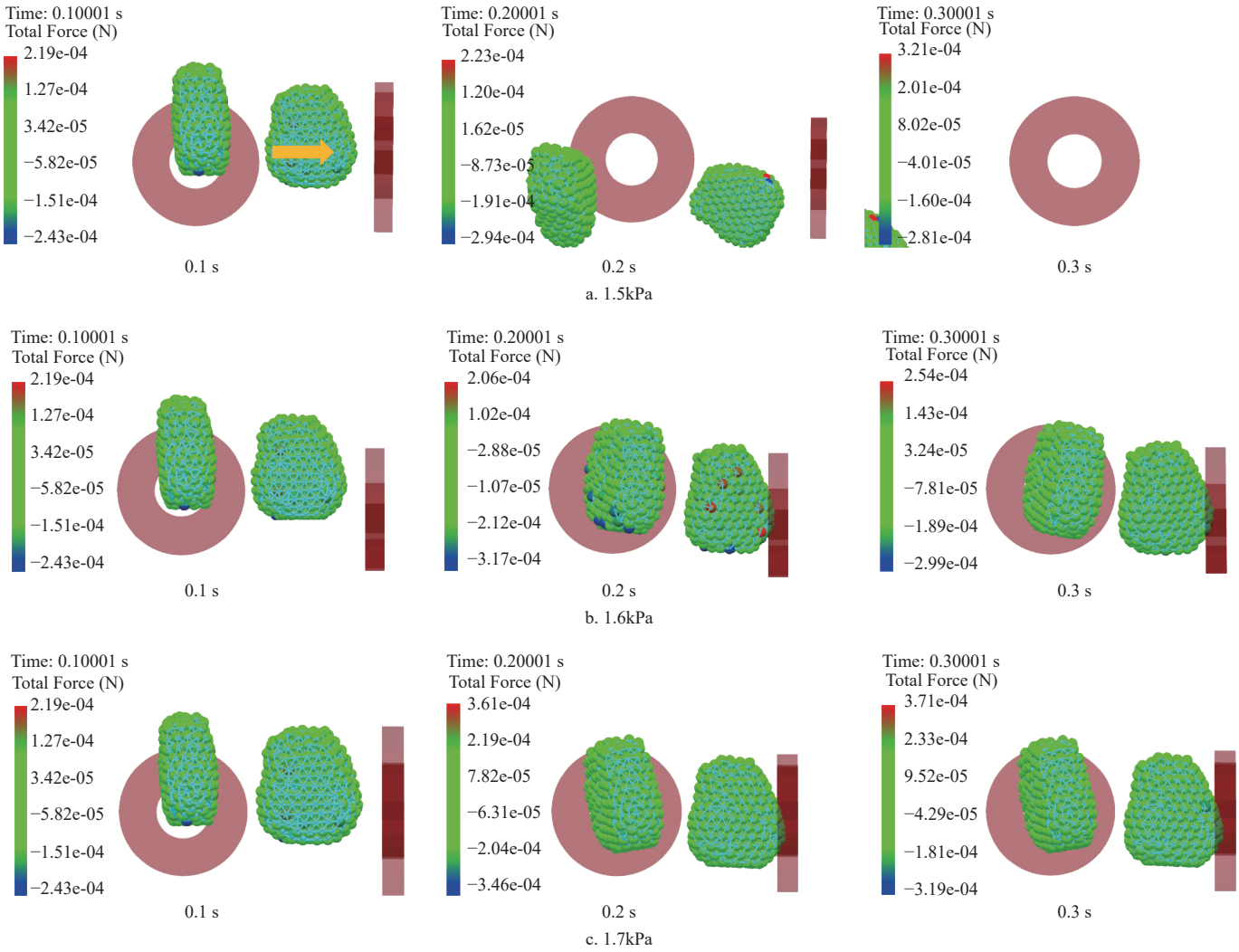

Figure 11 Simulation process of adsorbing horse tooth shape maize by the elastic suction seed pad

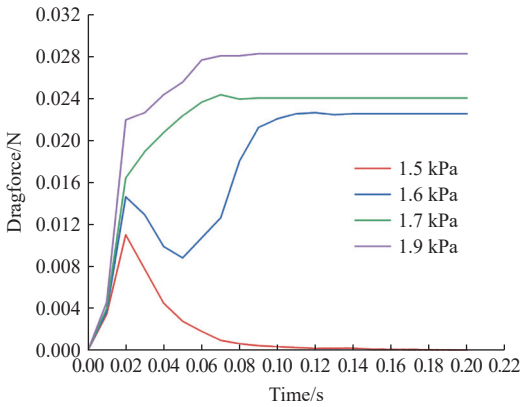

Figure 12 Comparison of the drag force exerted on the horse tooth maize model

Figure 11a shows that at a critical vacuum of 1.5 kPa, the maize kernels are produced and dropped down due to gravity. However, the distance between the seeds and the suction seed pad remains unchanged, and there is not much change in the suction force of the seed towards the suction seed. The seed suction mat did not absorb any seeds during the seed suction simulation. Increasing the critical vacuum and continuing the simulation is recommended to resolve this. When the critical vacuum was raised to 1.6 kPa, the distance between the seeds decreased gradually while falling. The suction force did not increase significantly until the seeds were stably adsorbed on the suction seed pad. Finally, the seed suction force stabilized at 3.54×10^{-4} N, as depicted in Figure 11b. When the critical vacuum was increased to 1.7 kPa, the distance quickly became smaller, the seeds were quickly adsorbed, and the suction force was also stabilized at 3.71×10^{-4} N, as shown in Figure 11c. To investigate the suction change of maize kernels under various critical vacuum conditions, we derived the suction force experienced by horse tooth maize during the falling process, as shown in Figure 12.

According to Figure 12, the drag force increases initially, then decreases and ultimately drops to zero when the critical vacuum is 1.5 kPa. When the critical vacuum is 1.6 kPa, the drag force increases initially, then decreases and finally increases. On the other hand, the drag force increases and remains stable when the critical vacuum is 1.7 and 1.9 kPa. Therefore, it is recommended that the critical vacuum during maize kernel transportation via seed suction disk should be greater than 1.7 kPa. Additionally, Figure 13 illustrates the analysis of suction force variation under 1.7 kPa critical vacuum conditions for the other four types of maize seeds. force. Spherical maize seeds are subjected to different forces than other shapes. Between 0.03 s to 0.06 s, the drag force acting on a spherical seed decreases rapidly. After 0.06 s, the head of the seed is closer to the suction hole, and the tail is farther away due to the small cross-sectional area of the head. As a result, the trailing force required for adsorption is smaller, and the seed changes its orientation. At this point, the head is adsorbed, indicating that

the spherical maize seed is more challenging to adsorb than other shapes.

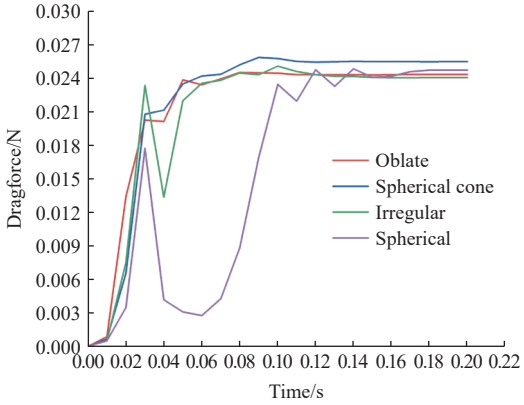

Figure 13 Comparison of the drag force exerted on the seed model

2.4.5 Effect of critical vacuum on picking seed process

If maize seeds experience resistance and friction from other seeds, collecting them with the seed success disk can be more challenging than carrying them. To address this issue, critical vacuum should be increased after studying the factors that affect the success of the suction disk suction. To demonstrate this, five different shapes of maize kernels will be moved at varying speeds, as depicted in Figure 14.

According to Figure 14, the drag force acting on irregular and spherical seeds initially increases, decreases, and eventually reaches a stable point. On the other hand, the drag force acting on oblate and spherical cone shapes first increases and then remains constant. Among all the shapes, the spherical cone experiences the highest drag. Based on the observations in Figure 14a, horse tooth maize seeds are primarily located in the lower left side of the seed suction disk's center. When fewer seeds obstruct the suction seed pad, it is easier for the pad to adsorb the seeds in direct contact with it. However, from Figure 14b and Figure 14c, it was noticed that the seed suction disk did not absorb spherical cone and spherical maize seeds, and most of the seeds were still in the population. Only a small number of particles were generated, and if they are adsorbed in this position, there is a higher chance of shedding. In Figure 14d, the suction disk successfully took oblate maize seeds since they were in direct contact with the suction seed disk and within the population. They were able to overcome the other seed's resistance. However, in Figure 14e, irregular seeds were scattered within the population and had less contact with the seed suction disk. The seeds in contact were not located at the suction pad suction opening location and did not seem to be taking seed. Several aspects must be considered to improve the success rate of taking seeds. Firstly, the seed number in the suction area should be reduced to mitigate the risk of falling due to other seed interference after the successful suction of the seed disk. Secondly, the critical vacuum should be increased to enhance the seed's ability to overcome resistance. Thirdly, increasing the number of times the seed contacts the seed suction disk can increase the vitality of its movement. This emphasizes the necessity of the seed-disturbing plate designed in this paper.

2.5 Performance experiment of metering seeds

2.5.1 Device and evaluation indicator

To enhance the performance of the seed-metering device, a maize seed-metering bench experiment was conducted in February 2023. As shown in Figure 15, the experimental device includes a frame, roller seed-metering, motor, motor governor, speed meter, air absorbing fan, fan governor, 12 VDC switching power supply adjustable monitoring transformer, and digital display gauge.

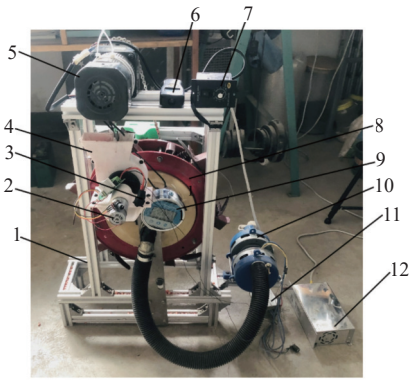

1. Frame 2. 12 V motor 3. 12 V motor forward and reverse button 4. Seed supply device 5. 220 V motor 6. Tachymeter 7. 220 V motor governor 8. Seed-metering device 9. Digital display gauge 10. Air absorbing fan 11. Fan governor 12. 12 VDC switching power supply adjustable monitoring transformer

Figure 15 Seed-metering experiment bench

The seed metering performance is measured using the qualified index, multiple indices, and missing index[21]. 250 maize seeds were counted sequentially and repeated three times. Equation (14) is used to calculate the performance index.

$$\begin{cases} Y_1 = \dfrac{n_1}{N'} \times 100\% \\ Y_2 = \dfrac{n_2}{N'} \times 100\% \\ Y_3 = \dfrac{n_3}{N'} \times 100\% \end{cases} \tag{14}$$

where, Y_1 is the qualified index, Y_2 is the multiple index, Y_3 is the missing index, n_1 is the single seed number, n_2 is the multi-seed number, n_3 is the empty seed number, N' is the theoretical seed number.

2.5.2 One-factor experiment

The seed working performance was affected by the seed layer height, the suction hole diameter, the critical vacuum, and the rotational speed of the seed disk. One-factor experiments were conducted to investigate their effect on the seed metering performance. The experimental arrangement is listed in Table 3.

Table 3 Single factor experimental arrangement

Level	Experimental factor			
	Seed layer height/mm	Critical Vacuum/kPa	Rotational speed of seed disk/ (r·min^{-1})	Suction hole Diameter/mm
1	20	2.00	10.0	4.0
2	28	2.41	14.1	4.5
3	40	3.00	20.0	5.0
4	52	3.59	25.9	5.5
5	60	4.00	30.0	

2.5.3 Multi-factor experiment

From the results of the single-factor experiment, the seed layer height was determined to range from 20 mm to 60 mm. The critical vacuum went from 2 to 4 kPa, the rotational speed of the seed disk ranged from 10 to 30 r/min, and the suction hole diameter was 4.5 mm. A multi-factor experiment was conducted with a five-level quadratic rotation orthogonal design to determine the optimal parameters, as listed in Table 4.

Table 4 Multi-factor experiment arrangement

Level	Experimental factor		
	Seed layer height X_1 (mm)	Critical vacuum X_2 (kPa)	Rotational speed of seed disk X_3 (r/min)
1	20	2.00	10.0
2	28	2.41	14.1
3	40	3.00	20.0
4	52	3.59	25.9
5	60	4.00	30.0

3 Results and discussion

3.1 Results of single factor experiment

Seed-metering performance was evaluated under different conditions. When the critical vacuum was 3 kPa, the seed disk's rotational speed was 20 r/min, and the suction hole diameter was 5 mm, the performance was observed under different seed layer heights, including 20 mm, 28 mm, 40 mm, 52 mm, and 60 mm, as shown in Figure 17a. Furthermore, when the seed layer height was 40 mm, the performance was conducted under different critical vacuum levels, including 2 kPa, 2.41 kPa, 3 kPa, 3.59 kPa, and 4 kPa, as shown in Figure 17b. In addition, when the seed layer height was 40 mm, the critical vacuum was 3 kPa, and the suction hole diameter was 5 mm, the seed-metering performance was evaluated under five different angular velocities of the seed disk, including 10 r/min, 14.1 r/min, 20 r/min, 25.9 r/min, and 30 r/min, as shown in Figure 17c. Lastly, when the seed layer height was 40 mm, the critical vacuum was 3 kPa, the rotational speed of the seed disk was 20 r/min, and the seed-metering performance was investigated under different suction hole diameters, including 4 mm, 4.5 mm, 5 mm, and 5.5 mm, as shown in Figure 17d.

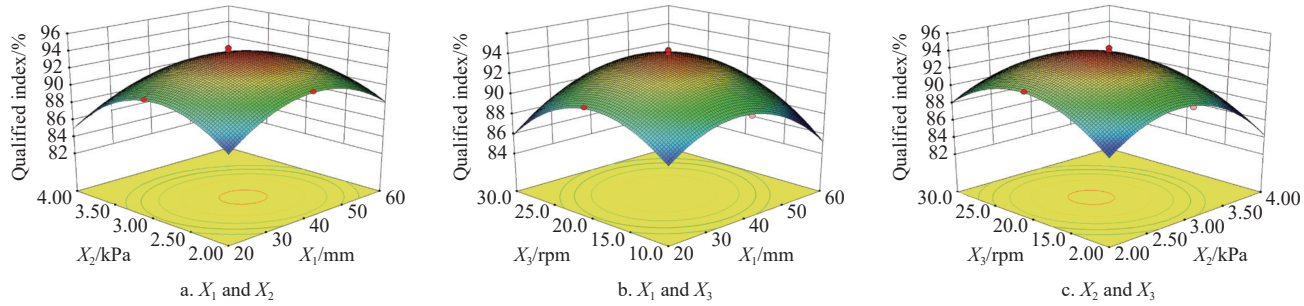

Figure 16 Impacts of interaction factor on the qualified index

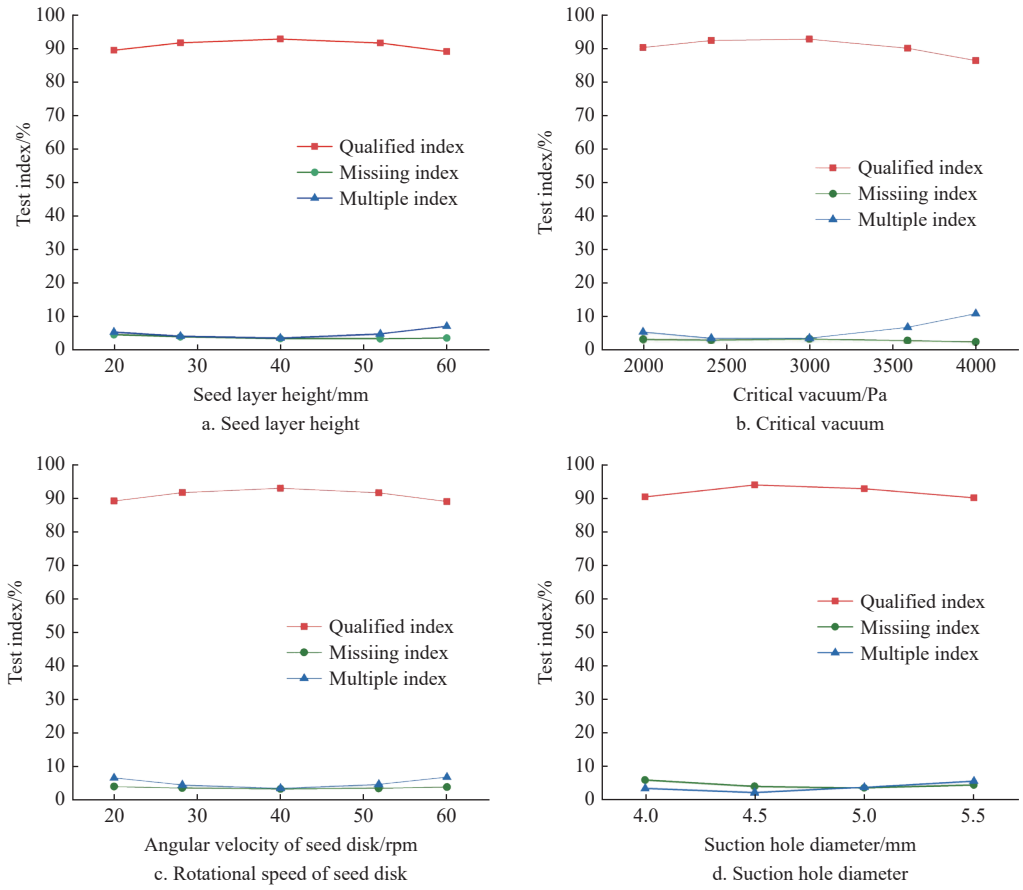

Figure 17 Influence of factors on seed metering performance

In Figure 17a, it is shown that the qualified index increased initially and then decreased as the seed layer height increased. Conversely, the missing and multiple indexes decreased initially and then increased, reaching their peak at a seed layer height of 40mm. The qualified index was 92.83%, while the missing and multiple indexes were 3.49% and 3.68%, respectively. Figure 17b

reveals that the qualified index increased initially and then decreased as the critical vacuum increased. Meanwhile, the missing index showed a gradual decrease, and the multiple indexes showed a gradual increase. The peak occurred at a vacuum of 3 kPa, corresponding to the qualified index of 92.83%, the missing index of 3.49%, and the multiple indices of 3.68%. In Figure 17c, the qualified index initially increased and then decreased, while the missing and multiple indexes displayed the opposite trend. The peak value occurred at an rotational speed of the seed disk of 20 r/min, corresponding to a qualified index of 92.83%, a missing index of 3.49%, and a multiple index of 3.68%. Finally, Figure 17d demonstrated that the qualified index first increased and then decreased, while the missing and multiple indexes first decreased and then increased. The highest values were observed at 4.5 mm, with the qualified index at 93.96%, the missing index at 3.99%, and the multiple index at 2.05%.

3.2 Results of multi-factor experiment

3.2.1 Analysis

The results of multi-factor experiments are listed in Table 5. The analysis of variance for results is listed in Table 6.

Table 5 Multi-factor experiments results

No.	Experimental factor			Performance index		
	Seed layer height X_1/mm	Critical vacuum X_2/kPa	Rotational speed of seed disk X_3/r·min^{-1}	Qualified index Y_1/%	Missing index Y_2/%	Multiple index Y_3/%
1	–1	–1	–1	90.98	5.13	3.89
2	1	–1	–1	90.53	4.73	4.74
3	–1	1	–1	89.61	4.26	6.13
4	1	1	–1	88.05	3.71	8.24
5	–1	–1	1	90.53	5.04	4.43
6	1	–1	1	91.19	4.49	4.32
7	–1	1	1	88.34	4.28	7.38
8	1	1	1	87.89	3.58	8.53
9	–1.682	0	0	90.71	5.17	3.58
10	1.682	0	0	89.96	4.15	5.89
11	0	–1.682	0	91.58	4.59	3.83
12	0	1.682	0	87.67	3.09	9.24
13	0	0	–1.682	89.92	4.69	5.39
14	0	0	1.682	90.41	4.6	4.99
15	0	0	0	93.93	4.06	2.01
16	0	0	0	93.54	4.05	2.41
17	0	0	0	94.42	4.11	1.47
18	0	0	0	94.03	4.01	1.96
19	0	0	0	93.86	4	2.14
20	0	0	0	94.34	3.95	1.71
21	0	0	0	94	3.84	2.16
22	0	0	0	93.7	3.9	2.4
23	0	0	0	93.8	4	2.2

The analysis of variance shows that the qualified index has a highly significant regression model (p<0.01). The interaction term X_2X_3 shows a non-significant effect (p>0.05). In contrast, the remaining factors show significant or highly significant effects. The lack of fit terms is also not significant (p=0.5003). Therefore, the regression equation of the qualified index was shown in Equation (15).

$$Y_1 = 93.96 - 0.22A - 1.17B - 0.029C - 0.28AB + 0.28AC - 1.31A^2 - 1.57B^2 - 1.37C^2 \quad (15)$$

Table 6 Variance analysis

Index	Source	Sum of square	Df	F-value	p-value
Qualified index Y_1	Model	115.98	9	163.64	<0.0001**
	X_1	0.69	1	8.71	0.0112*
	X_2	18.55	1	235.54	<0.0001**
	X_3	0.011	1	0.15	0.7088
	X_1X_2	0.62	1	7.82	0.0151*
	X_1X_3	0.62	1	7.82	0.0151*
	X_2X_3	0.34	1	4.27	0.0593
	X_1^2	27.47	1	348.84	<0.0001**
	X_2^2	38.96	1	494.75	<0.0001**
	X_3^2	30.04	1	381.46	<0.0001**
	Residual	1.02	13		
	Lack of fit	0.38	5	0.95	0.5003
	Pure error	0.64	8		
	Cor total	117.01	22		
Missing index Y_2	Model	5.66	9	133.90	<0.0001**
	X_1	1.12	1	239.21	<0.0001**
	X_2	2.71	1	577.32	<0.0001**
	X_3	0.026	1	5.46	0.0362*
	X_1X_2	0.011	1	2.40	0.1455
	X_1X_3	0.011	1	2.40	0.1455
	X_2X_3	0.006	1	1.29	0.2767
	X_1^2	0.88	1	188.42	<0.0001**
	X_2^2	0.046	1	9.88	0.0078**
	X_3^2	0.84	1	180.04	<0.0001**
	Residual	0.061	13		
	Lack of fit	0.005	5	0.15	0.9733
	Pure error	0.056	8		
	Cor total	5.72	22		
Multiple index Y_3	Model	120.79	9	120.72	<0.0001**
	X_1	4.55	1	40.95	<0.0001**
	X_2	35.44	1	318.73	<0.0001**
	X_3	0.071	1	0.64	0.4374
	X_1X_2	0.79	1	7.14	0.0192*
	X_1X_3	0.46	1	4.14	0.0627
	X_2X_3	0.25	1	2.27	0.1561
	X_1^2	15.99	1	143.87	<0.0001**
	X_2^2	42.72	1	384.26	<0.0001**
	X_3^2	21.54	1	193.70	<0.0001**
	Residual	1.45	13		
	Lack of fit	0.69	5	1.46	0.3025
	Pure error	0.76	8		
	Cor total	122.24	22		

Note: * represents a significant difference (p<0.05); ** represents an extremely significant difference (p<0.01).

The analysis of variance also shows that the regression model of the missing index is highly significant (p<0.01). The interaction terms X_1X_2, and X_1X_3, X_2X_3 show a non-significant effect (p>0.05). The remaining factors show significant or highly significant effects. The lack of fit terms is also not substantial (P=0.9733). Therefore, the regression equation for the missing index is shown in Equation (16).

$$Y_2 = 3.99 - 0.29A - 0.45B - 0.043C + 0.24A^2 - 0.054B^2 + 0.23C^2 \quad (16)$$

The analysis of variance also shows that the regression model of the multiple indices is highly significant (p<0.01). The interaction terms X_1X_3, X_2X_3 show a non-significant effect (p>0.05). In comparison, the remaining factors show significant or highly

significant effects. The lack of fit terms is also not substantial (p=0.9733). Therefore, the regression equation for the multiple index was shown in Equation (17).

$$Y_3 = 2.05 + 0.58A + 1.61B + 0.072C + 0.31AB + A^2 + 1.64B^2 + 1.16C^2 \quad (17)$$

3.2.2 Influence of factors on the qualified index

The response surfaces for the seed layer height, the critical vacuum and the rotational speed of the seed disk affecting the qualified index was constructed using Design-Expert 8.0.6t, as shown in Figure 16.

From Figure 16a, we can find that the qualified index follows a rising and falling pattern as the critical vacuum increases. Similarly, the qualified index follows a similar rising and falling trend as the seed layer height increases. The maximum value occurs when the seed layer height is between 20 and 60 mm, and the critical vacuum is between 2-4 kPa. Figure 16b shows that the qualified index follows a rising and falling pattern as the rotational speed of the seed disk increases while maintaining a critical vacuum of 3 kPa. Similarly, the qualified index follows a similar rising and falling trend as the seed layer height increases. The maximum value occurs when the seed layer height is between 20-60 mm and the rotational speed of the seed disk is between 10-30 r/min. From Figure 16c, the qualified index follows a rise and fall as the rotational speed of the seed disk increases while maintaining a seed layer height of 40 mm. Similarly, the qualified index follows a similar rising and falling trend as the critical vacuum level increases. The maximum value occurs when the critical vacuum is between 2-4 kPa and the rotational speed of the seed disk is between 10-30 r/min.

3.2.3 Parameter optimization and validation

To determine the optimal working parameters, a regression model is developed. The objective function and constraint conditions were as follows.

$$F_{max} = Y_1 - Y_2 - Y_3 \quad (18)$$

$$\text{s.t.} \begin{cases} Y_1 \geq 80.0\% \\ Y_2 \leq 8.0\% \\ Y_3 \leq 15.0\% \\ 20\ \text{mm} \leq X_1 \leq 60\ \text{mm} \\ 2\ \text{kPa} \leq X_2 \leq 4\ \text{kPa} \\ 10\ \text{rpm} \leq X_3 \leq 30\ \text{rpm} \end{cases} \quad (19)$$

F_{max} served as the ultimate optimization objective. We used the optimization module provided by Design-Expert 8.0.6 to obtain the optimal solution. The results showed that when the seed layer height was set at 40 mm, and the critical vacuum was maintained at 2.85 kPa, and the rotational speed of the seed disk was 20.1 r/min, the qualified index reached a value of 94.15%, with a corresponding missing index of 4.09% and a multiple index of 1.76%.

To verify the reliability of the optimization results, an experiment was conducted. The experiment results are that the qualified index is 93.79%, the missing index is 4.02%, and the multiple index is 2.19%. Seed metering operation was reliable and stable during the experiment. It shows the close agreement between the actual and theoretical optimization results.

4 Conclusions

A seed-metering device with elastic suction pad was developed for better seed extraction and bump resistance. After conducting a force analysis of the seed-metering process of the seed-metering device, the factors affecting seed-metering performance were identified and addressed. Using Fluent software, six different suction hole diameters were simulated to determine the range. From the results it is clear that the maximum pressure and the highest velocity is observed when the diameter is 4.5 mm. With EDEM-FLUENT method, a maize seed suction experiment was conducted to determine the critical vacuum of five shape types of maize seeds. The result show that their critical vacuum conditions are more than 1.7 kPa, and the trailing force required for adsorption is smaller. Also found the seed number in the suction area should be reduced to mitigate the risk of falling after the successful suction of the seed disk, and the critical vacuum should be increased to enhance the seed's ability to overcome resistance, and increasing the times between seeds and the suction disk can increase the vitality of its movement.

The single-factor bench experiments were conducted to determinate the range of 4 factors. The result shows that the seed layer height is 20-60 mm, and the critical vacuum is 2-4 kPa, and the rotational speed of the seed disk is 10-30 r/min, and the 4.5 mm suction hole diameter is suitable. Further, A three-factor, five-level quadratic rotational orthogonal experiment was conducted to optimize the parameters. From the results, we can see that when the seed layer height was 40 mm, and the critical vacuum was 2.85 kPa, and the rotational speed was 20.1 r/min, the qualified index was 94.15%, and the missing index was 4.09%, and the multiple indices was 1.76%. The verification experiment results show that under the same condition, the qualified index is 93.79%, the missing index is 4.02%, and the multiple indices is 2.19%. The results align closely, and the optimization findings are reliable.

Acknowledgements

National Natural Science Foundation of China (Grant No. 52065004, 52365030); Lanzhou Municipal Young Talent Innovation Project (Grant No. 2023-QN-146); Major Cultivation Project of Collegiate Scientific Research and Innovation Platform of Gansu Provincial Department of Education (2024CXPT-15); Special Project of Gansu Provincial Commissioner for Science and Technology (23CXGA0066); Gansu Agricultural Machinery R&D, Manufacturing and Promotion Application in 2023 Integrated Pilot Project (3-3).

[References]

[1] Shi L R, Wu J M, Sun W, Zhang F W, Sun B G, Liu Q W, et al. Simulation test for metering process of horizontal disc precision metering device based on discrete element method. Transactions of the CSAE, 2014; 30(8): 40–48. (in Chinese)

[2] Liu J, Cui T, Zhang D X, Yang L, Shi S. Mechanical-pneumatic combined corn precision seed-metering device. Transactions of the CSAM, 2012; 43(2): 43–47. (in Chinese)

[3] Gao X J, Zhou J H, Lai Q H. Design and experiment of pneumatic cylinder precision seed-metering device for panax notoginseng. Transactions of the CSAE, 2016; 32(2): 20–28. (in Chinese)

[4] Li Y H, Yang L, Zhang D X, Cui T, Zhang K L, Xie C J, Yang R M. Analysis and test of linear seeding process of maize high speed precision metering device with air suction. Transactions of the CSAE, 2020; 36(9): 26–35. (in Chinese)

[5] Yang L, Shi S, Cui T, Zhang D X, Gao N N. Air-suction corn precision metering device with mechanical supporting plate to assist carrying seed. Transactions of the CSAM, 2012; 43(Z1): 48–53. (in Chinese)

[6] Chen J, Li Y M. Study on seeds movement law in sowing test stand with suction and vibration. Transactions of the CSAM, 2002; 33(1): 47–50. (in Chinese)

[7] Li L. A preliminary study on the theory and experimentation of the suction-type metering device for precision drill. Transactions of the CSAM, 1979;

9(3): 56–63. (in Chinese)

[8] Yan B X, Zhang D X, Yang L, Cui T, Zhong X J, Li Y H. Performance analysis of gravity assist filling precision seed-metering device with synchronously rotating seed plate and vacuum chamber. Transactions of the CSAM, 2018; 49(S1): 117–124. (in Chinese)

[9] Yang W, Fang X F, Li J D, Li C X. Design and experiment of air-suction precision seed meter with self-clearing seed chamber for corn plot test. Transactions of the CSAM, 2019; 50(6): 64–73. (in Chinese)

[10] Yan B X, Zhang D X, Cui T, He X T, Ding Y Q, Yang L. Design of pneumatic maize precision seed-metering device with synchronous rotating seed plate and vacuum chamber. Transactions of the CSAE, 2017; 33(23): 15–23. (in Chinese)

[11] Shi L R, Zhao W Y, Yang X P, Sun B G, Sun W. Design and test of metering device with forced seeding and opening for corn direct seeding machine. Transactions of the CSAM, 2018; 49(2): 41–47. (in Chinese)

[12] Tang H, Xu F D, Xu C X, Zhao J L, Wang J W. The influence of a seed drop tube of the inside-filling air-blowing precision seed-metering device on seeding quality. Computers and Electronics in Agriculture, 2023; 204: 107555.

[13] Zhu T. Research on pneumatic-mechanical compound peanut precision seed-metering device. Xinjiang, China: Shihezi University. 2021. (in Chinese)

[14] He S. Analysis and experiment on the adsorption mechanism of the perturbation pneumatic precision seed metering device for rapeseed. Anhui, China: Anhui Agricultural University, 2021. (in Chinese)

[15] Shi L R, Sun B G, Zhao W Y, Yang X P, Xin S L, Wang J X. Optimization and test of performance parameters of elastic air suction type corn roller seed-metering device. Transactions of the CSAM, 2019; 50(10): 88–95, 207. (in Chinese)

[16] Shi L R, Zhao W Y, Yang X P. Effects of typical corn kernel shapes on the forming of repose angle by DEM simulation. Int J Agric & Biol Eng, 2022; 15(2): 248–255.

[17] Ding L, Yang L, Zhang D X, Cui T, Gao X J. Design and experiment of seed plate of corn air suction seed metering device based on DEM-CFD. Transactions of the CSAM, 2019; 50(5): 50–60. (in Chinese)

[18] Cui T, Liu J, Yang L, Zhang D X, Zhang R, Lan W. Experiment and simulation of rolling friction characteristic of corn seed based on high-speed photography. Transactions of the CSAE, 2013; 29(15): 34–41. (in Chinese)

[19] Tang H, Zhu G X, Xu W L, Xu C S, Wang J W. Discrete element method simulation of rice grains impact fracture characteristics. Biosystems Engineering, 2024; 237: 50–70.

[20] Wu M C, Cong J L, Yan Q, Zhu T, Peng X Y, Wang Y S. Calibration and experiments for discrete element simulation parameters of peanut seed particles. Transactions of the CSAE, 2020; 36(23): 30–38. (in Chinese)

[21] GB/T 6973-2005; Testing methods of single seed drills. Precision Drills: Beijing, China, 2005. (in Chinese)